STABILITY OF CO_2-BRINE PRIMARY DRAINAGE

H. Ott* and S. Berg
Shell Global Solutions International BV, The Netherlands.

This paper was prepared for presentation at the International Symposium of the Society of Core Analysts held in Aberdeen, Scotland, UK, 27-30 August 2012

ABSTRACT
A viscous unstable displacement can lead to viscous fingering and to enhanced channeling in rock heterogeneities. The viscous stability of the CO_2-brine primary drainage process is therefore of major importance for CO_2 sequestration in saline aquifers and determines the spread of the CO_2 plume in the target aquifer and consequently the initial utilization of the pore space for storage. In previous papers [1,2] we presented some experimental results of CO_2-brine displacement in sandstone and a stability analysis of the experimental situation. In the present study we investigate the onset of viscous fingering in a parameter range relevant for sandstone aquifers, thereby studying under which conditions CO_2-brine displacement remains stable on the experimental and field scales. Our findings are not limited to CO_2-brine systems, but can be applied to most two-phase flow problems in reservoir engineering.

INTRODUCTION
During immiscible displacement in porous media, viscous fingering can be observed when the displacing phase has a greater mobility than the displaced phase. This is due to the viscous pressure gradient, which is steeper in the displaced phase ahead of the finger (perturbation) than at the base of the displacement front; this causes the finger to grow [3].
In principle, the stability of the primary drainage process is sensitive to the following parameters: (1) viscosity ratio (we consider μ_{brine}/μ_{CO2}=10 to 40 to be a reasonable range for CO_2 sequestration), (2) Corey exponents (we vary n_{brine} and n_{CO2} between 2 and 5 which we consider reasonable for sandstones), and (3) the CO_2 end point at residual water saturation. These parameters are systematically varied in the present study. We discuss the base case with neutral buoyancy ($\Delta\rho$=0) and with zero capillary pressure (p_C=0) by using a Buckley-Leverett approach to determine mobility ratios and verify the resulting stability by numerical simulations. We successively introduce capillarity and gravity into numerical simulations to establish criteria for the displacement stability. Finally, we carry out an up-scaling step from the experimental scale to the field scale.

DISPLACEMENT STABILITY FOR ZERO p_C AND GRAVITY
In single-phase flow and two-phase flow in Hele-Shaw cells, the fluid mobility is simply the viscosity, and the criterion for viscous instability is the viscosity ratio $M=\mu_1/\mu_2>1$,

where 1 and 2 refer to the displaced and displacing phase, respectively. In a porous medium, the fluid mobility is reduced by the relative permeability ($k_r(S_w)$), and the fluid mobility $k_r(S_w)/\mu$ is therefore a function of fluid saturation. The open question now is how to evaluate the mobility ratio in this situation.

Several authors argue that the $k_r(S_w)$ endpoints should be used to assess stability (see e.g. [4]). For the so-called end-point mobility ratio (M_e) the relative permeabilities of the displacing and displaced phases are evaluated at a location far upstream and far downstream, respectively. As a consequence, the criterion for the onset of instability does not depend on the concrete form of the relative-permeability saturation function, but only on the respective endpoint phase permeability. Others use the position of the shock front that is typical of immiscible displacement in order to evaluate stability, but there is no consensus about the exact form of the mobility ratio. The intuitive form is the shock-front mobility ratio that is obtained by evaluating the fluid mobility of the displacing phase directly behind the shock front and of the displaced phase ahead of it:

$$M_{SF} = \frac{k_{r,CO2}\left(S_{W,SF}\right)/\mu_{CO2}}{k_{r,brine}\left(S_W = 1\right)/\mu_{brine}} > 1 \qquad (1)$$

This follows a similar logical reasoning as for the liquid-liquid interface in a Hele-Shaw cell, for which this criterion was rigorously derived by linear stability analysis. The main difference between M_e and M_{FS} is that M_e indicates instability for far more situations than M_{FS} does, and that the prediction by M_e is independent of $k_r(S_w)$ details such as the curvatures.

Another method that is used by some authors to evaluate the mobility ratio at the shock front position is the total shock-front mobility ratio (see e.g. [5]):

$$M_{TSF} = \frac{k_{r,CO2}\left(S_{W,SF}\right)/\mu_{CO2} + k_{r,brine}\left(S_{W,SF}\right)/\mu_{brine}}{k_{r,brine}\left(S_W = 1\right)/\mu_{brine}} > 1. \qquad (2)$$

Other forms of M_{TSF} are also discussed in the literature (see e.g. [6]). These different forms of mobility ratio are used to evaluate displacement stability for various physical reasons, but the actual form of the stability criteria often appears to be influenced by mathematical convenience to arrive at an elegant analytical solution.

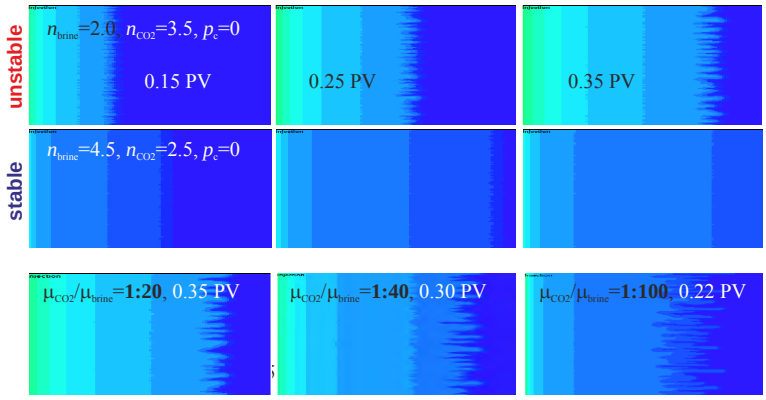

Figure 1: Time series of finger growth for the unstable situation (upper row) and stable situation (middle row). Lower row: Fingering pattern for viscosity ratios 1:20, 1:40 and 1:100 with p_C=0.

What is missing in the whole discussion is a realistic substantiation of the stability criteria. In this paper we present the stability criteria by comparing the various analytical expressions with numerical modeling based on experimental results. We then upscale this from the experimental scale to the field scale. The simulations were performed with the Shell proprietary reservoir simulator *MoReS*, which is a fully implicit finite volume Darcy flow simulator. We used the experimental flow geometry grid properties and flow conditions reported in [1,2] in 2D. At this point we merely note that the instabilities were triggered by a 4% random variation of the permeability field initialized for each simulation run, and that the robustness was tested in some cases by refining the grid size by factors of 2x2 and 4x4. Fig. 1 shows a time series of an unstable (upper row) and a stable displacement (middle row). In contrast to the unstable displacement pattern, in stable displacement the small perturbations do not grow with time. Fingering patterns for different viscosity ratios are shown in the lower row in Fig. 1.

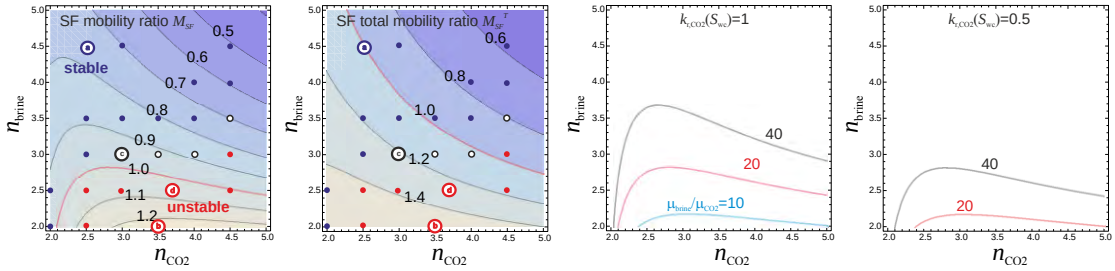

Figure 2: Shock-front mobility ratio M_{FS} (left) and total shock-front mobility ratio $M_{FS,T}$ (second) for primary drainage at p_C=0. The data are plotted as a function of Corey exponents n_{CO2} and n_{brine} for μ_{brine}/μ_{CO2}=20. The stability assessments by numerical simulations at individual points in the stability map are shown as dots: blue corresponds to stable displacement and red to unstable. At some positions (white dots) it could not clearly be determined whether the displacement is stable or not.

Fig. 2 compares the results of the numerical simulations (dots) with the stability map as calculated for M_{SF} (left) and M_{TSF}. Even with the uncertainties close to the stability border (M=1), the numerical results are in a reasonable agreement with M_{SF}, and even show an opposite trend to M_{TSF} (as M_e does not depend on the Corey exponents). From this we conclude that $M_{SF} > 1$ is a criterion for viscous fingering. The two images on the right in Fig. 2 show the stability line for different viscosity ratios and for two different CO_2 end points. The largest areas of stability are found for lower viscosity ratios and lower CO_2 end points.

INFLUENCE OF $p_C > 0$ ON THE LABORATORY SCALE

So far we have not taken capillary pressure into account, even though capillarity is known to suppress fingering, particularly on short length scales. We showed earlier [1] that on the experimental scale (~10cm scale), p_C already stabilizes the flood front at low capillary pressures corresponding to an IFT in the order of 0.1 to 1mN/m (see also Fig. 5). For an IFT that is realistic for CO_2-brine systems (30mN/m), it has been found that the displacement is stable for all scenarios in the envelope of the parameter space used in this study. The up-scaling to field scale will be discussed further below.

EFFECT OF GRAVITY

When we consider the actual density of CO_2 and brine, it is evident that significant changes could occur in the vertical and horizontal saturation profiles that develop during displacement. In Fig. 3 we compare a simulation of an unstable situation without density difference (upper left image) with one showing the actual density difference at 50°C and 100bar (upper middle image). With the generally lower density of CO_2, the plume makes an upward migration leading to a larger saturation jump at the top of the simulation domain (compared to the middle of the domain and to the no-gravity case), but also to a depletion of CO_2 at the bottom of the simulation domain.

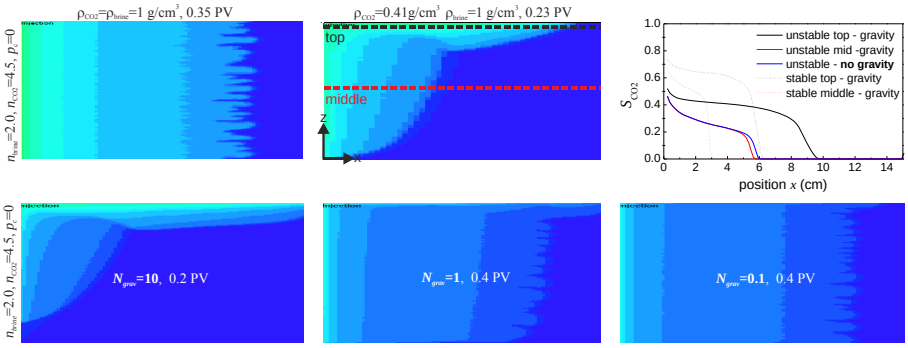

Figure 3: Unstable displacement without gravity (top left) and with gravity (top middle). The plot on the top right shows the CO_2 saturation profiles along the line indicated in the top middle figure. Lower row: Displacement with the influence of gravity for different injection rates, resulting in different gravity numbers N_{grav}=10, 1, 0.1.

As a result, the already unstable case becomes even more destabilized at the top of the domain, but is stabilized at the bottom. This leads to a self-amplification of the gravity tongue and to suppression of the individual fingers that are present in the no-gravity case. The increased shock front height at the top can even lead to unstable situations, whereas the no-gravity case suggests stable displacement.

The relative significance of gravitational forces to viscous forces is reflected in the gravity number [7,8]:

$$N_{grav} = \frac{Kg\Delta\rho}{\mu v}. \qquad (3)$$

To visualize the transition from a gravity-dominated to a viscous-dominated unstable system, we performed simulations at different flow rates while varying N_{grav} between 10 and 0.1. The results are shown in the lower row of Fig. 3. Whereas at $N_{grav} >> 1$ gravity overrun dominates the displacement profiles, at $N_{grav} << 1$ gravity can be ignored and individual fingers form. At $N_{grav} \sim 1$ characteristic features of both regimes are found. Fig. 4 shows 3D simulations on core scale (left and middle) and on field scale (right). As in the no-gravity case, the flood front turns stable when a realistic capillary pressure is introduced, and the pronounced gravity tongue for p_C=0 turns into a slightly tilted flood front. However, on the field scale (right image), the flood front is highly unstable even with a realistic p_C.

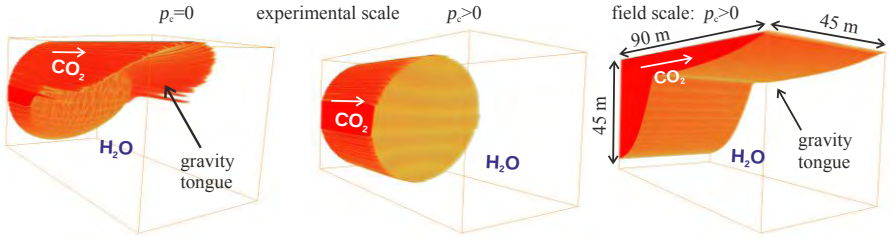

Figure 4: Gravity overrun in the cylindrical geometry of the core flood experiment for n_{brine}=2.0, n_{CO2}=3.5, $k_{r,CO2}(S_{w,c})$=0.5 endpoint and a viscosity ratio of 1:20. Left: p_C =0, middle: realistic p_C - at a realistic capillary pressure, the gravity tongue is suppressed. Right: Simulation on field scale for the same settings and the realistic p_C, but with $k_{r,CO2}(S_{w,c})$=1. The gravity tongue is the dominating feature.

DISPLACEMENT STABILITY ON THE FIELD SCALE

As pointed out earlier, capillarity only stabilizes flow on short length scales, i.e. on the experimental scale. The associated length scale is the scale of the p_C-induced gradients, and so we do not expect that p_C will stabilize the flood front on the field scale.

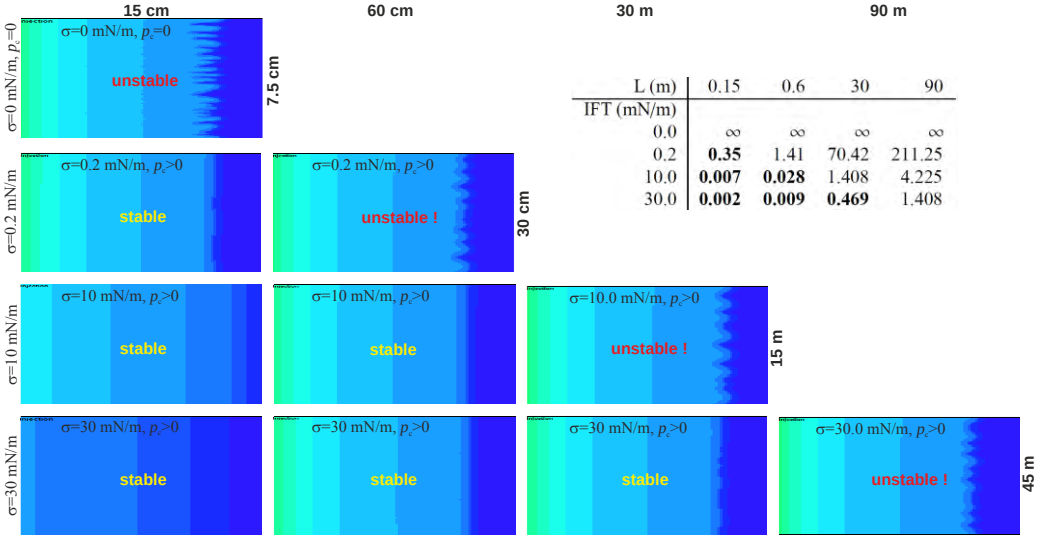

L (m)	0.15	0.6	30	90
IFT (mN/m)				
0.0	∞	∞	∞	∞
0.2	**0.35**	1.41	70.42	211.25
10.0	**0.007**	**0.028**	1.408	4.225
30.0	**0.002**	**0.009**	**0.469**	1.408

Figure 5: Increasing p_C leads to stabilization on short length scales only. A condition that is unstable on short length scales with p_C=0 is also unstable on large length scales with a realistic p_C. The linear flow velocity is kept constant at v=2.96 10^{-6} m/s. The inset table shows $N_{M,cap}$ for the different simulations.

A systematic up-scaling is presented in Fig. 5: the length scale is varied from left to right and p_C from top (p_C=0) to bottom (realistic p_C) by scaling IFT. For up-scaling purposes, IFT is increased until the flood front appears stable on the given length. Subsequently, the dimension of the modeling domain was increased to the scale at which fingering is observed again at the same linear flow velocity (1ft/day) and at the given IFT. For the realistic CO_2-brine IFT of 30mN/m, unstable displacement is found on a transversal length scale of 45m, i.e., on the relevant field scale. This is plausible since we know that fingering is caused by the mobility contrast at the shock front. Capillarity smoothens the shock front on a length scale l_{cap} that is set by capillary dispersion, but the shock front

appears sharp again on a scale $L >> l_{cap}$, at which point we again observe the fingering pattern.
The correlation between the length scale and the stabilizing effect of p_C suggests that the onset of fingering should be scaled with the macroscopic capillary number, N_{cap}, which is explicitly length scale dependent [7]:

$$N_{M,cap} = \frac{\mu v L}{p_C K}. \quad (3)$$

Here, L is the length scale of observation which also sets the pressure gradient. Hence, $N_{M,cap}$ can be understood as the ratio of the scale of observation to the width of the capillary smear-out. The table of capillary numbers versus L and IFT is shown in Fig. 5. This shows that stability is consistent when $N_{M,cap} < 1$, whereas viscous fingering was found when $N_{M,cap} > 1$. We fully reproduced the stability map in Fig. 2 on field scale with p_C taken into account, and this clearly shows that p_C stabilizes the flood front on short length scales only.

SUMMARY

For primary drainage we have identified the following criteria for viscous fingering: a shock front mobility ratio $M_s > 1$ and a macroscopic capillary number $N_{M,cap} > 1$. The endpoint mobility ratio M_e and the total shock front mobility ratio M_{TSF} do not describe the numerical observations. A realistic capillary pressure stabilizes the CO_2-brine displacement on the experimental scale, i.e. on a scale of a few centimeters, for the parameter range, corresponding to CO_2 injection in sandstone aquifers. However, on the field scale the above-mentioned instability criteria apply again.
Generally this also holds where gravitational forces are relevant, but gravity must be taken into account when calculating M_s and $N_{M,cap}$, because the simple 1D Buckley-Leverett shock front argument is no longer valid in a gravity-dominated system where $N_{grav} >> 1$. In CO_2 sequestration, the self-amplifying nature of the gravity overrun ("gravity tongue") in unstable displacement might lead to substantial bypassing of the reservoir volume even if the CO_2-brine system is only moderately unstable (M_s always < 1.5).

REFERENCES

* Corresponding author; E-mail address: holger.ott@shell.com, research@holger-ott.de
1. H. Ott, S. Berg, S. Oedai, Society of Core Analysts, SCA2011-05 (2011).
2. S. Berg, S. Oedai, and H. Ott, Int. J. o. Greenhouse Gas Control, available online (2011).
3. J. Van Wunnik and K. Wit, 1st European Conference on the Mathematics of Oil Recovery, University of Cambridge (1989).
4. G. I. Barenblatt, V. M. Entov, V. M. Ryzhik, Theory of Fluid Flow Through Natural Rocks, Kluwer, Dordrecht (1990).
5. J. Hagoort, SPE Journal 14(1) 63–74 (1974).
6. A. Riaz, H. A. Tchelepi, Transport in Porous Media 64 315–338 (2006).
7. L. Anton and R. Hilfer, Physical Review E 59(6) 6819–6823 (1999).
8. A. Riaz, H. A. Tchelepi, Phys. Fluids 16(12) 4727–4737 (2004).